www.MaterialsViews.com

ADVANCED
ENERGY
MATERIALS
www.advenergymat.de

FULL PAPER

Supramolecular Polymerization Promoted In Situ Fabrication of Nitrogen-Doped Porous Graphene Sheets as Anode Materials for Li-Ion Batteries

Wei Ai, Jian Jiang, Jianhui Zhu, Zhanxi Fan, Yanlong Wang, Hua Zhang, Wei Huang,* and Ting Yu*

A novel strategy of utilizing supramolecular polymerization for fabricating nitrogen doped porous graphene (NPG) with high doping level of 12 atom% as the anode material for lithium ion batteries is reported for the first time. The introduction of supramolecular polymer (melamine cyanurate) functions not only as a spacer to prevent the restacking of graphene sheets but also as a sacrificial template to generate porous structures, as well as a nitrogen source to induce in situ N doping. Therefore, pores and loose-packed graphene thin layers with high N doping level are very effectively formed in NPG after the annealing process. Such highly desired structures immediately offer remarkably improved Li storage performance including high reversible capacity (900 mAh g^{-1} after 150 cycles) with good cycling and rate performances. The effects of annealing temperature and heating rates on the final electrochemical performance of NPG are also investigated. Furthermore, the low cost, facile, and scalable features of this novel strategy may be helpful for the rational design of functionalized graphene-based materials for diverse applications.

1. Introduction

Developing green and efficient energy storage techniques is undoubtedly crucial for a sustainable world.[1] Lithium ion batteries (LIBs) are just such kind of devices that have been extensively exploited as the primary power source for portable electronics.[2] The rapid development of portable electronics and the ever-increasing demand for energy, especially the emergence of electric vehicles, require high performance LIBs with breakthroughs on energy and power densities.[3] Currently, the mostly used commercial anode is graphite with unfortunately low Li intercalation capacity (372 mAh g^{-1} ideally) and poor rate capability.[4] Therefore, considerable efforts have been afforded into finding alternative carbon-based anode materials that can be applied in advanced energy storage.[5] Among various carbon-based materials, porous carbon is the most promising one owing to its large surface area and high porosity with unique transport properties.[6] Indeed, an improved Li storage capacity is achieved in porous carbon as a benefit of the forming pores, which could act as the active sites for Li storage.[7] Beyond that, the Li storage property of porous carbon can be further enhanced via minimizing the thickness of carbon layer to fewer-layer graphene so that Li ions can be absorbed on both sides of graphene sheets according to the falling card model.[8] Unfortunately, it is still a great challenge to fabricate highly conductive porous carbon with single or few layer graphene sheets and high porosity at the same time.

Graphene, a miracle material in materials science, has attracted intensive research interests for energy-related applications due to its atomically thin 2D geometrical structure and prominent intrinsic physical and chemical features.[9] The LIBs performance of graphene was first investigated by Honma

W. Ai, Prof. W. Huang
Key Laboratory of Flexible Electronics (KLOFE) and Institute of Advanced Materials (IAM)
National Jiangsu Synergetic Innovation Center for Advanced Materials (SICAM)
Nanjing Tech University (NanjingTech)
30 South Puzhu Road, Nanjing 211816, China
E-mail: iamwhuang@njtech.edu.cn
W. Ai, Dr. J. Jiang, Dr. J. Zhu, Y. Wang, Prof. T. Yu
Division of Physics and Applied Physics
School of Physical and Mathematical Sciences
Nanyang Technological University
637371, Singapore
E-mail: yuting@ntu.edu.sg

Z. Fan, Prof. H. Zhang
School of Materials Science and Engineering
Nanyang Technological University
639798, Singapore
Prof. W. Huang
Key Laboratory for Organic Electronics and Information Displays (KLOEID) and Institute of Advanced Materials (IAM)
Nanjing University of Posts and Telecommunications
Nanjing 210023, Jiangsu, China
Prof. T. Yu
Department of Physics
Faculty of Science
National University of Singapore
117542, Singapore

**ADVANCED
ENERGY
MATERIALS**

www.advenergymat.de

www.MaterialsViews.com

FULL PAPER

and co-workers in 2008.[10] Although a reversible capacity of 540 mAh g^{-1} was observed at a current density of 50 mA g^{-1}, it did not display exciting cycling stability. Since then, graphene has aroused great enthusiasm in exploiting its potential applications as the anode for LIBs.[11] Nevertheless, the irreversible restacking or aggregation of graphene sheets due to the strong π–π stacking and van der Waals interaction between graphene sheets usually results in the following disadvantages: (i) The loss of active sites for Li accommodation, such as nanopores and edge-type sites;[12] (ii) the breakdown of connected channels for fast electron and ion transport;[13] and (iii) the degradation of inherent properties for individual sheets, such as large theoretical specific surface area.[14] Conversely, further structural engineering of graphene by heteroatom doping or organic functionalization can significantly improve its Li storage property.[5a,15] So far, nitrogen is the most abundantly investigated heteroatom owing to its diverse precursors (e.g., NH$_3$, urea, melamine, and cyanamide), and relative easy to induce N doping into carbons as they are two neighboring elements.[16] Generally, in situ doping (e.g., chemical vapor deposition and direct carbonization) and post-treatment are the most routinely used methods to fabricate nitrogen doped graphene.[17] However, the complex and time-consuming synthesis procedures of in situ doping result in low production yield and high cost,[18] whereas post-treatment usually suffers from inevitable aggregation of graphene sheets.[19] Besides, the low N doping level (<10%) can only lead to a limited progress on enhancing the electrochemical performance.[20] Based on the above considerations, high performance electrode materials are expected for example by designing single or few-layer graphene constructed porous structure with a high N doping level. It will be certainly great if such interesting and promising 2D based structures could

be synthesized through processing- and economical-friendly way.

In this work, we present a novel strategy toward the above goal and successfully demonstrate a simple yet very effective approach for in situ fabrication of nitrogen-doped porous graphene (NPG) by using a supramolecular polymer (melamine cyanurate (MC), chemical structure shown in **Figure 1**a) as both N source and pore-forming agent. The post annealing process decomposes the sacrificial MC component and releases a large amount of N containing gases, which induce N doping and simultaneously generate porous structure. Benefiting from the unique porous architecture and high N doping level, the NPG materials exhibit impressive electrochemical performances when applied as the anode materials for LIBs. Furthermore, this low cost and facile method could be suitable for mass production, which implies the great potential of the NPG materials for advanced energy storage.

2. Results and Discussion

The NPG materials were synthesized by a novel two-step methodology (Figure 1b). In the first step, graphene oxide@melamine cyanurate composite (GO@MC) was synthesized by supramolecular polymerization. First, melamine was dissolved into the GO solution and spontaneously absorbed on the GO layers through π–π interaction.[21] Then, cyanuric acid was added into the mixture. The hydrogen-bond between melamine and cyanuric acid induces a supramolecular polymerization,[22] causing the formation of GO@MC. In the second step, GO@MC was subjected to annealing treatment at different temperatures (higher than the maximum thermal decomposition of MC
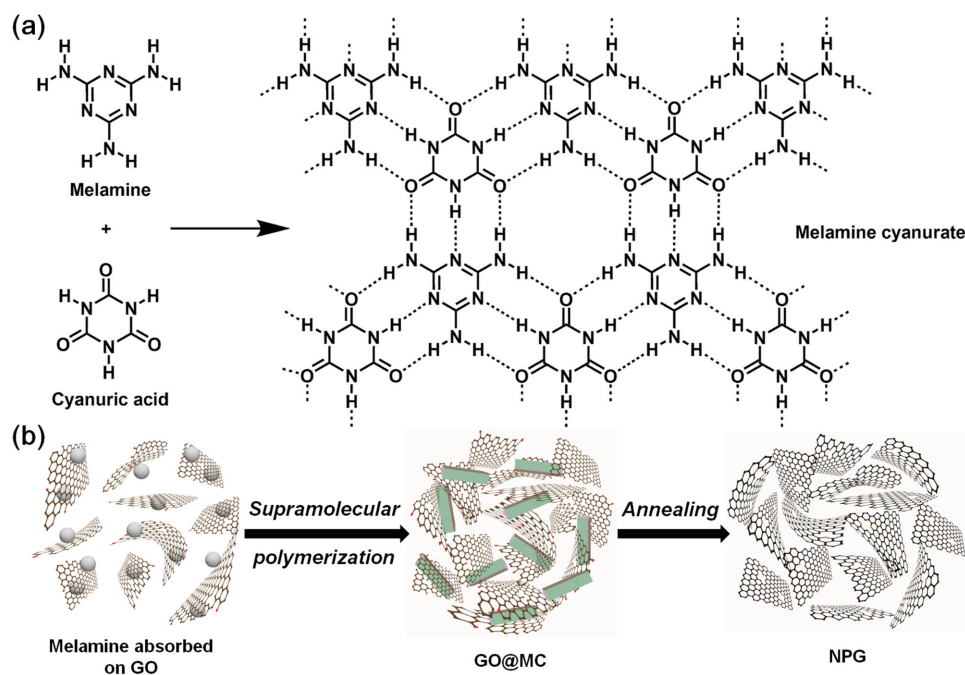

Figure 1. a) Supramolecular polymerization of melamine and cyanuric acid results in the formation of MC. b) Schematic illustration of the synthesis procedure of NPG materials.
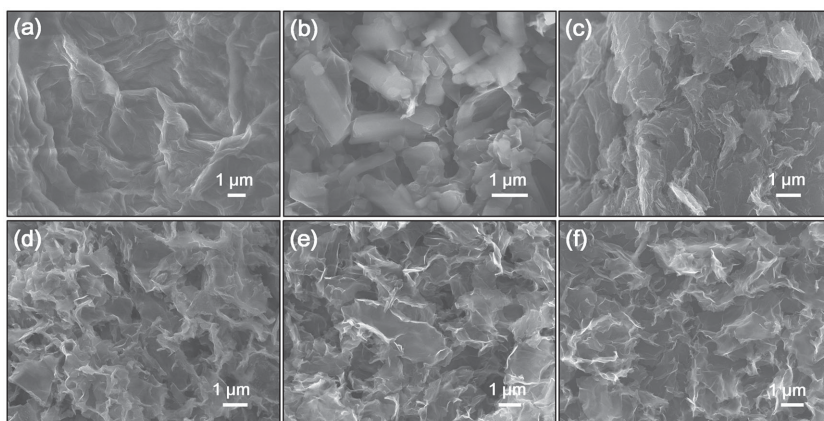
www.MaterialsViews.com

ADVANCED
ENERGY
MATERIALS
www.advenergymat.de

FULL PAPER

Figure 2. FESEM images of a) GO, b) GO@MC, c) G-650, d) NPG-450, e) NPG-650, and f) NPG-850.

porous structure with the diameters ranging from submicrometer to few micrometers. By contrast, the thermally reduced graphene oxide (G-650) prepared in the absence of MC tends to aggregate, forming a graphite-like structure (Figure 2c). Meanwhile, no pores are observed in G-650, demonstrating the importance of MC for effectively preventing the restacking of graphene sheets and promoting the formation of pores. The complete decomposition of MC and successful formation of graphene thin layers constructed porous structure after the annealing process can also be readily observed by TEM images (**Figure 3**a). These features would facilitate the accessibility of electrolyte and shorten the diffusion length of Li ions, which could be advantageous for Li storage. In addition, the recovery of graphitic carbon structures can guarantee fast electron transportation, as displayed in the high-resolution TEM (HRTEM) image of NPG-650 (Figure 3b). Moreover, scanning transmission electron microscopy (STEM) with the corresponding elemental mapping images (Figure 3c–e) reveals that nitrogen is homogenously distributed in graphene sheets.

Nitrogen adsorption–desorption technique was also used to investigate the porous structure of NPG materials. **Figure 4**a reveals that the isotherms of these materials show close to type IV (G-650 and NPG-650) and type II (NPG-450 and NPG-850) patterns according to the IUPAC classification.[25] The obtained pore structure parameters of these materials are summarized in **Table 1**. Remarkably, the Brunauer–Emmett–Teller (BET) surface area of NPG materials (106–152 m^2 g^{-1}) is larger than G-650 (69 m^2 g^{-1}) and the directly thermal annealed GO with melamine (6 m^2 g^{-1}),[19] indicating the introduction of MC can

(≈410 °C)). During this process, the decomposition of sacrificial MC component releases a large amount of nitrogen containing gas (e.g., NH_3, HCN, and HNCO) from the interlayer space of graphene sheets,[23] which consequently produces substantial internal stresses, leading to the expansion of graphene sheets to single or few-layer with porous structures. Simultaneously, the removal of thermally labile oxygen functional groups from graphene sheets induces active sites for in situ N doping, which finally results in the formation of NPG materials (labeled as NPG-T, where T is the pyrolysis temperature). It should be mentioned that this strategy is conceptually different and in fact superior to the previous ones as evidenced by the remarkably improved performance. In the previous works, polymers or ionic liquid was annealed together with GO and carbonized, which eventually leads to the formation of graphene-based composites.[24] On clear contrast, our proposed process could completely decompose supramolecular MC and yield a pure N doped graphene, which is particularly appealing since it provides an exclusive opportunity for investigating whether graphene is a potential valid alternative anode for next generation LIBs.

To evaluate the proposed strategy and unveil the properties of our products, systematic characterizations are performed. The materials were first studied by field-emission scanning electron microscopy (FESEM) and transmission electron microscopy (TEM). The morphology of GO is flaky texture, leading to a rippled or wrinkled structure (**Figure 2**a). FESEM image of GO@MC (Figure 2b) shows that the rod-like MC supramolecular crystals with an average size of 1.45 μm × 560 nm are wrapped by GO sheets. Notably, these supramolecular crystals disappeared in the FESEM images of NPG materials after the annealing process. As shown in Figure 2d–f, NPG-450, NPG-650, and NPG-850 exhibit a crumpled and loose-packed thin layer morphology. The overlapping and interconnecting of graphene sheets result in the formation of
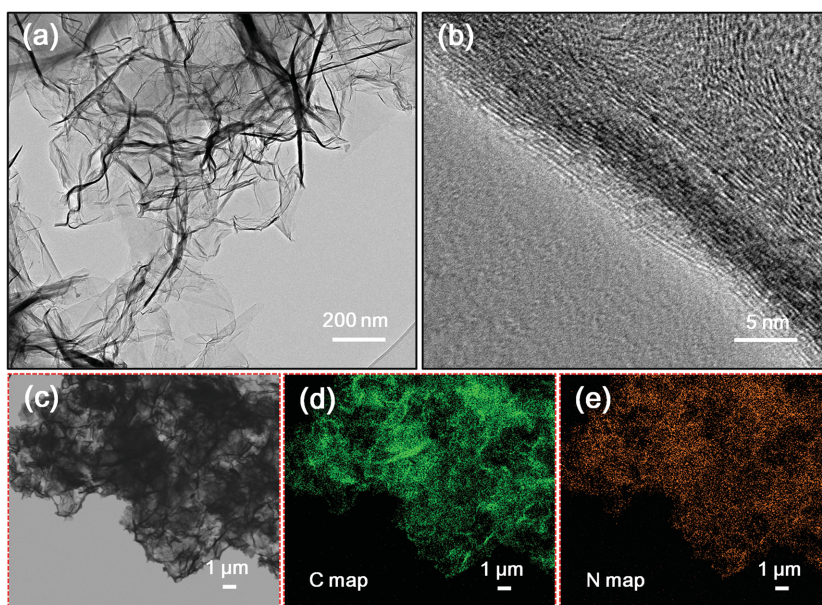

Figure 3. a) TEM and b) HRTEM images of NPG-650. c) STEM image of NPG-650 with the corresponding d) carbon and e) nitrogen elemental mapping images.
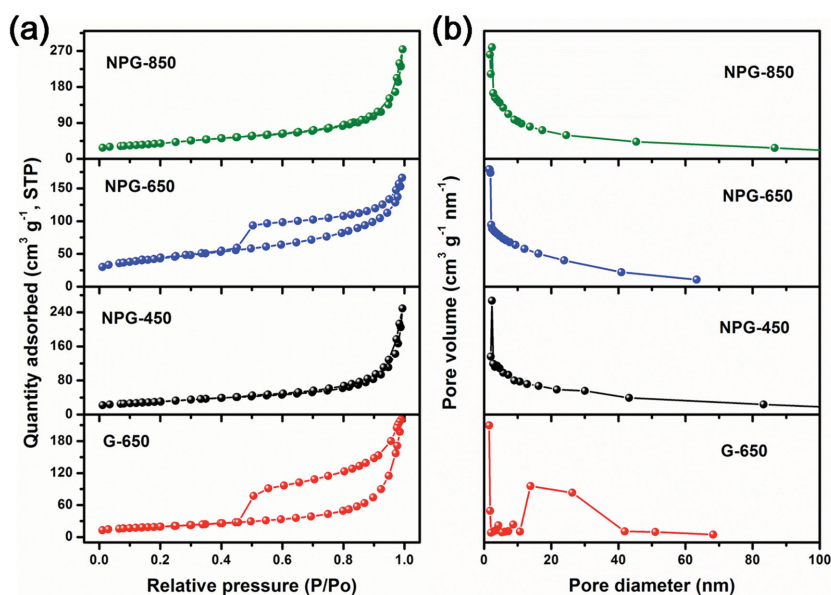
Figure 4. a) Nitrogen adsorption–desorption isotherms and b) the corresponding pore size distribution of G-650, NPG-450, NPG-650, and NPG-850.

diffraction peak located at $2\theta = 11.2°$ with an interlayer spacing of 0.79 nm, which is assigned to the (002) plane of graphite due to the intercalation of oxygen functional groups in between the graphite layers.[26] For G-650 and NPG materials, the removal of oxygen functional groups from graphene sheets makes this peak up-shifted to ≈26.2°, corresponding to an interlayer spacing of 0.34 nm. It is worth noting that G-650 presents a well-defined peak, whereas NPG materials display a broad hump-shaped peak, once again demonstrating the disordered graphene phases in NPG materials. Comparing with NPG-450 and NPG-650, the diffraction peak of NPG-850 is more defined and evidently shifts to a larger angle, which suggests its higher graphitization degree. Moreover, the increased I_D/I_G ratio in the Raman spectra of NPG materials (Figure S1b, Supporting Information) also illustrates their disordered feature that caused by the porous structure and N doping induced structural distortion in the graphene sheets.[27] To analyze the elemental composition and their chemical status in the samples, XPS measurements were carried out. The survey scan of GO (**Figure 5**a) shows the presence of C and O atoms located at ≈285 and 532 eV, with an atomic percentage of 40.9% and 50.1%, respectively.[5a,28] However, the O content in G-650 and NPG materials is dramatically decreased, which suggests the reduction of GO after the annealing treatment. In addition, the N 1s peak located at ≈399 eV is observed in NPG materials, clearly implying the successful doping of graphene with N atom.[19] The N content in NPG-450, NPG-650, and NPG-850 is calculated to be 18.8 at%, 12.0 at%, and 8.9 at%, respectively. Figure 5b–d presents the high-resolution N 1s spectra of NPG materials. The deconvoluted peaks located at ≈398.4, 399.8, and 401.3 eV could be successively ascribed to the pyridine-like N, pyrrole-like N, and graphite-like N.[18b] It is found that pyridine-like N is the primary N bonding state in NPG materials as shown in Table S1 (Supporting Information). Theoretical calculations demonstrate that the pyridine-like N is mostly favorable for Li storage due to its stronger binding energy with Li, along with lower Li diffusion and desorption barrier.[29]

effectively prevent the restacking of graphene sheets, which is in good agreement with previous FESEM and TEM results. Compared to the theoretical value of graphene (2630 m^2 g^{-1}), the relative low surface area of NPG must due to the existence of few-layer graphene sheets in its unusual structure. Additionally, it is also found that the BET surface area of NPG materials is dependent on the annealing temperature. As shown in Table 1, the BET surface area of NPG materials increases from 106 to 152 m^2 g^{-1} with increasing the annealing temperature from 450 to 650 °C but decreases to 136 m^2 g^{-1} at 850 °C, which probably owing to the higher graphitization degree in NPG-850 as demonstrated by X-ray diffraction (XRD) results (see below). Pore size distribution curves (Figure 4b) reveal that the NPG materials have a multimodal pore distribution. It should be noted that NPG-650 has the largest BET surface area but the smallest pore volume, which implies the existence of large amounts of micro- and mesopores in NPG-650 structure. The high surface area, large pore volume, and plentiful pores of NPG-650 can not only facilitate the accessibility of electrolyte but also provide additional active sites for Li storage.

Further structural information about the NPG materials was obtained from XRD, X-ray photoelectron spectroscopy (XPS), and Raman spectroscopy. XRD pattern of GO (Figure S1a, Supporting Information) shows a characteristic

To evaluate the potential of NPG materials as anode for LIBs, we fabricated a series of coin-type cells following the standard half-cell configuration. As shown in **Figure 6**a and Figure S2a–c (Supporting Information), both G-650 and NPG materials show similar cyclic voltammogram (CV) curves that belong to typical carbon-based anodes.[5a,15a] During the first cycle, a reduction peak in the potential range of 0.3–0.9 V is clearly detected, which is ascribed to the formation of a solid electrolyte interphase (SEI) layer on the electrode surface caused by electrolyte decomposition.[5b,c] In the subsequent cycles, the disappearance of this SEI formation peak together with the almost overlapped CV curves imply the formation of a stable SEI layer after the first cycle. Two weak peaks are also observed during the first CV curve of NPG-850 in the potential range of 1.5–2.5 V (Figure S2c, Supporting Information), which should

Table 1. Pore structure parameters of G-650, NPG-450, NPG-650, and NPG-850.

Sample	BET surface area [m^2 g^{-1}]	Total pore volume [cm^3 g^{-1}]	Average pore diameter [nm]
G-650	69	0.24	14.0
NPG-450	106	0.25	9.78
NPG-650	152	0.20	5.2
NPG-850	136	0.30	8.7

www.MaterialsViews.com

ADVANCED
ENERGY
MATERIALS
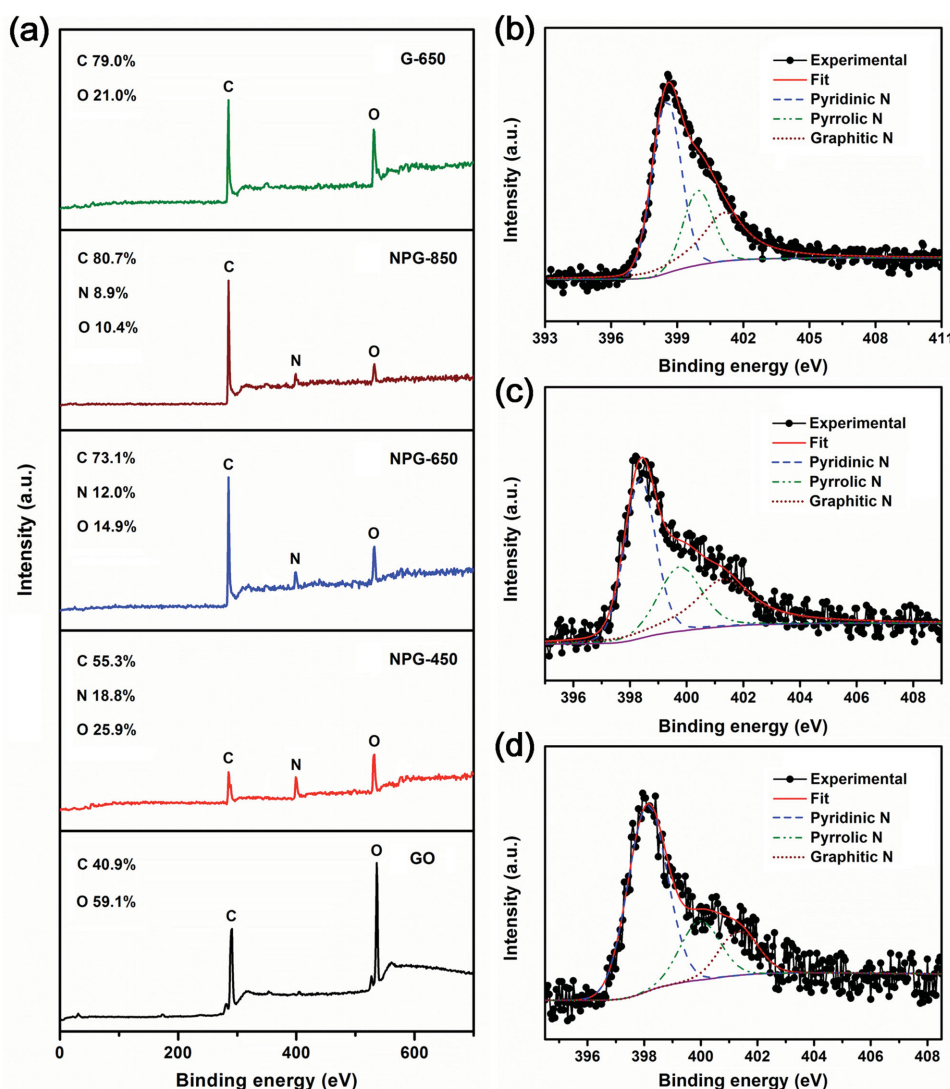www.advenergymat.de

FULL PAPER

Figure 5. a) XPS survey spectra of GO, G-650, NPG-450, NPG-650, and NPG-850. High-resolution N 1s XPS spectra of b) NPG-450, c) NPG-650, and d) NPG-850.

be related to the Li trapped in the irreversible sites that is associated with high temperature induced collapse of the pores.[30] Figure 6b and Figure S2d–f (Supporting Information) depict the galvanostatic charge–discharge curves of the materials at 0.2 C (1 C corresponds to a current density of 372 mA g^{-1}). It can be seen that the first discharge curves show a sloping plateau at ≈0.7 V, indicative of the formation of SEI layer,[5a–c] which matches well with the CV results. The first discharge capacity of G-650, NPG-450, NPG-650, and NPG-850 is 1025, 1381, 1440, and 1167 mAh g^{-1}, corresponding to a coulombic efficiency of 52.2%, 37.7%, 55.3%, and 51.8%, respectively. The large irreversible capacity loss is attributed to the SEI formation that is commonly observed in carbon-based anodes. However, the coulombic efficiency of these materials increases dramatically in the following cycles, as shown in Figure S3 (Supporting Information).

The cycling performance of these materials is investigated under the same current density of 0.2 C (Figure 6c). Evidently,

NPG-650 electrode exhibits substantially higher capacity than the other three electrodes throughout the whole cycles. The reversible capacity of NPG-650 electrode is 900 mAh g^{-1} after 150 cycles, over two times larger than the theoretical value of graphite (372 mAh g^{-1}), and far larger than the value of G-650 (516 mAh g^{-1}), NPG-450 (313 mAh g^{-1}), and NPG-850 (563 mAh g^{-1}). The gradually increase of capacity upon cycling can be assigned to the electrochemical activation process, which results in an improved accessibility of Li ions into the inner area of the electrode, thus more activated sites for Li storage.[5a,b,15b] More significantly, the NPG-650 electrode also shows superior rate capability. As illustrated in Figure 6d and Figure S4 (Supporting Information), NPG-650 electrode always delivers higher capacity than the other electrodes with current density increasing from 0.2 to 10 C. The reversible capacities of NPG-650 electrode are 723, 631, 566, 501, 418, and 356 mAh g^{-1}, at 0.2, 0.5, 1, 2, 5, and 10 C, respectively. These values are competitive with the other recently reported graphene-based
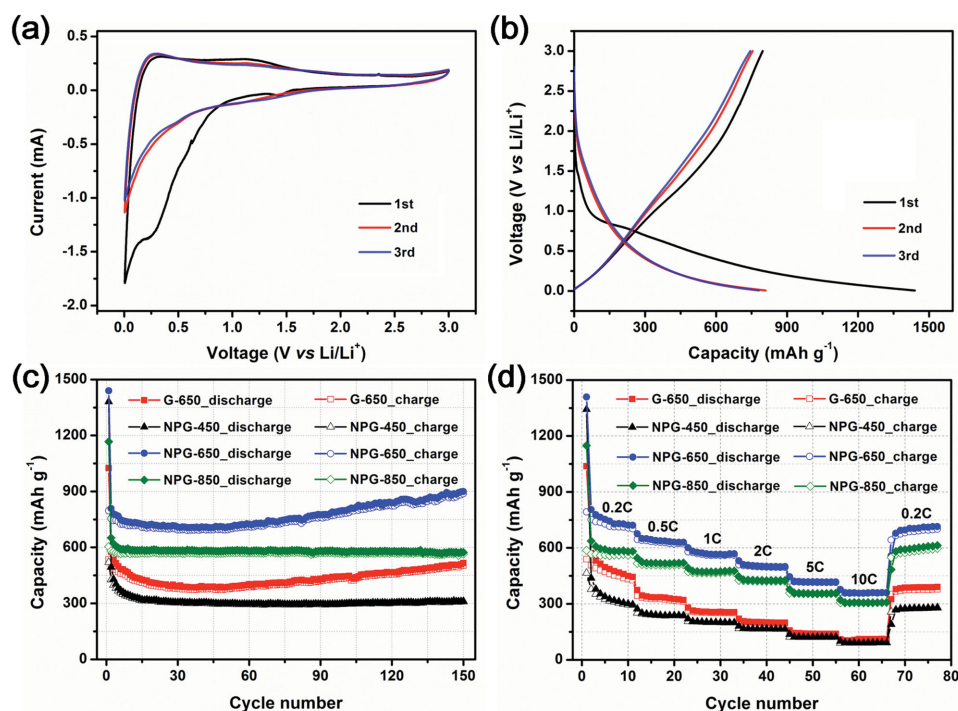
Figure 6. a) CV curves of the NPG-650 electrode at a scanning rate of 0.5 mV s^{-1} in the voltage range of 0.005–3 V (vs Li/Li$^+$). b) Galvanostatic charge–discharge curves of the NPG-650 electrode at a current density of 0.2 C. c) Cycling performance of the G-650, NPG-450, NPG-650, and NPG-850 electrodes at a current density of 0.2 C. d) Rate performance of the G-650, NPG-450, NPG-650, and NPG-850 electrodes at different current densities.

anode materials, such as phosphorus-doped graphene,[15a] edge-selectively halogenated graphene,[31] and mesoporous graphene.[32] Moreover, even after deep cycling at 10 C, the capacity of NPG-650 electrode can be recovered to its initial value when the current density is restored to 0.2 C, indicating its excellent reversibility.

Considering different heating rate may result in different pore structures in the NPG materials, we further investigated the influence of heating rate on the final electrochemical performance. Figure S5 (Supporting Information) shows the FESEM images of NPG-650′ (prepared at a heating rate of 20 °C min^{-1}). It is interesting to note that NPG-650′ also has a porous structure that consisted of crumpled and loose-packed graphene thin layers, showing no much difference from that of NPG-650 (Figure 2e). Meanwhile, the electrochemical performance of NPG-650′ (Figure S6, Supporting Information) is also comparable to NPG-650, implying the Li storage property of NPG materials is independent on the heating rate. Electrochemical impedance spectroscopy (EIS) was employed to investigate the kinetic behavior of the electrochemical reaction (**Figure 7**). The data fitted from the semicircle at high frequency region by using the equivalent circuit (inset of Figure 7) reveals that the charge transfer resistance (R_{CT}) of G-650, NPG-450, NPG-650, and NPG-850 is 78, 116, 42, and 52 Ω, respectively, which suggests NPG materials with N doping and porous structure possess higher electrolyte accessibility and better charge transport capability than G-650. The relative high R_{CT} of NPG-450 is due to its low reduction degree, as demonstrated by previous XPS and XRD results. At low frequency range region, the straight lines with larger phase angles, evidencing lower

Li-ion diffusion resistance in NPG materials compared with G-650.

The outstanding electrochemical performance of NPG materials mainly originates from their unique porous architecture and high N doping level. On one hand, the high surface area and porous structure are favorable for electrolyte accessibility and fast Li diffusion throughout the electrode material.[5b,27b] With this design, the as-formed mesopores can also act as "cavities" for further Li storage, which additionally contributes to the remarkable electrochemical properties.[11a,32] In particular, the
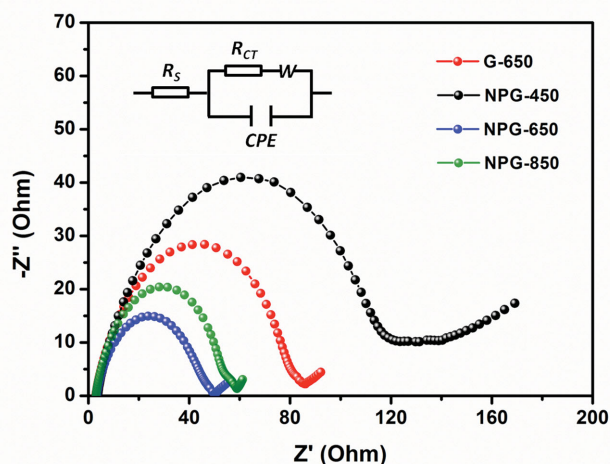

Figure 7. Nyquist plots of the G-650, NPG-450, NPG-650, and NPG-850 electrodes. Inset is the equivalent circuit model.

graphene thin layers with corrugated and interconnected structure can greatly increase Li ions adsorption, shorten Li ions diffusion length, and facilitate electron transportation.[5a,32] On the other hand, N doping further enhances the conductivity of graphene sheets, whereas the doping induced topological defects are beneficial for Li accommodation.[15a,18a] All of these merits lead to the final outstanding electrochemical performance. It is also noted that the electrochemical performance of NPG materials highly depend on the annealing temperature. 650 °C is the ideal temperature that can ensure the as-obtained NPG material has high N content and good conductivity, as well as appropriate porous structure, thus superior Li storage capacity (that is, capacity of NPG-650 > NPG-850 > NPG-450). Further increasing the annealing temperature will induce lower N doping content and porosity (NPG-850), while decreasing the annealing temperature will result in poor reduction degree (NPG-450), both of which are disadvantageous for Li storage performance.

3. Conclusion

In summary, we have demonstrated a novel chemical approach to prepare NPG by using a supramolecular polymer (MC) as the nitrogen source and pore-forming agent. The successful realization of graphene thin layers constructed porous structure with high N doping level mainly arises from the introduction of sacrificial MC template, which can effectively prevent graphene restacking and simultaneously promote pore formation and N doping by releasing a large amount of N containing gases during the annealing process. With this design, NPG exhibits exceptional electrochemical performance in terms of high reversible capacity (900 mAh g^{-1} after 150 cycles) with good cycling and rate performances, highlighting it might be a promising candidate for high performance LIBs. We also demonstrate that the annealing temperature is a key step for the final electrochemical performance of NPG materials since it has significant impact on the N doping level and porous structure. More importantly, this simple strategy might be helpful for the rational design of functionalized graphene-based materials for advanced energy storage.

4. Experimental Section

Preparation of GO: GO was synthesized from natural graphite (China Jixi Jinyu Graphite Co., Ltd) by a modified Hummers' method as described in previous work.[28b]

Preparation of NPG Materials: 400 mg GO was dispersed in 100 mL deionized water by ultrasonication for 2 h and subsequently centrifuged at 1000 rpm for 5 min to remove the unexfoliated particles. Then, 562 mg melamine was dissolved in the GO dispersion under stirring at 80 °C. Afterward, 38 mL of freshly prepared 15 mg mL^{-1} cyanuric acid solution was dropwised into the mixture and then stirred at 80 °C for 1 h. The obtained product was collected by hot filtration, washed with deionized water for several times, and dried in an oven at 90 °C. Finally, the sample was annealed under Ar atmosphere at a flow of 100 cm^3 min^{-1} with a heating rate of 5 °C min^{-1} to pyrolysis temperature (450, 650, and 850 °C) for 2 h.

Preparation of Reduced rGO: rGO was prepared by annealing GO powder at 650 °C under the same experimental parameters.

Characterization: XPS analysis was carried out on an ESCALAB MK II instrument. XRD analysis was measured on a Rigaku D/max-IIIB diffractometer with Cu Kα radiation (λ = 1.54184 Å). Raman spectra were collected using a WITEC CRM200 Raman system equipped with 532 nm laser source. FESEM and TEM images were performed on a JEOL JSM-6700F and JEOL JEM-2010, respectively. Nitrogen adsorption–desorption isotherms were obtained using a Micromeritics Tristar II.

Electrochemical Characterizations: Electrochemical properties of the materials as anode for LIBs were investigated in 2032 coin-type cells. The working electrodes were prepared by mixing active material, poly (vinylidene fluoride) binder and acetylene black in a weight ratio of 8:1:1 to form a slurry. Then, the slurry was pasted on a copper foil and dried at 100 °C in vacuum overnight to remove the solvent. The mass loading of electrode material on the current collector is approximately 1 mg. Coin cells were assembled in argon-filled glove box using Li metal foil as the counter electrode, and 1 M LiPF$_6$ in a 1:1 (w/w) mixture of ethylene carbonate and dimethyl carbonate as the electrolyte. Electrochemical tests were performed in the voltage range of 0.005–3 V (vs Li/Li$^+$) using a NEWARE battery testing system. CV measurements and EIS were performed on CHI 760D electrochemical workstation.

Supporting Information

Supporting Information is available from the Wiley Online Library or from the author.

[1] P. Poizot, F. Dolhem, *Energy Environ. Sci.* **2011**, *4*, 2003.

[2] Y. G. Guo, J. S. Hu, L. J. Wan, *Adv. Mater.* **2008**, *20*, 2878.

[3] J. M. Tarascon, M. Armand, *Nature* **2001**, *414*, 359.

[4] H. Nishihara, T. Kyotani, *Adv. Mater.* **2012**, *24*, 4473.

[5] a) W. Ai, Z. Luo, J. Jiang, J. Zhu, Z. Du, Z. Fan, L. Xie, H. Zhang, W. Huang, T. Yu, *Adv. Mater.* **2014**, *26*, 6186; b) L. Qie, W. M. Chen, Z. H. Wang, Q. G. Shao, X. Li, L. X. Yuan, X. L. Hu, W. X. Zhang, Y. H. Huang, *Adv. Mater.* **2012**, *24*, 2047; c) J. Sun, H. Liu, X. Chen, D. G. Evans, W. Yang, X. Duan, *Adv. Mater.* **2013**, *25*, 1125; d) J. Jiang, J. Zhu, W. Ai, Z. Fan, X. Shen, C. Zou, J. Liu, H. Zhang, T. Yu, *Energy Environ. Sci.* **2014**, *7*, 2670.

[6] a) P. Adelhelm, Y. S. Hu, L. Chuenchom, M. Antonietti, B. M. Smarsly, J. Maier, *Adv. Mater.* **2007**, *19*, 4012; b) F. Bonino, S. Brutti, P. Reale, B. Scrosati, L. Gherghel, J. Wu, K. Mullen, *Adv. Mater.* **2005**, *17*, 743.

[7] a) K. Sato, M. Noguchi, A. Demachi, N. Oki, M. Endo, *Science* **1994**, *264*, 556; b) N. Takami, A. Satoh, T. Ohsaki, M. Kanda, *Electrochim. Acta* **1997**, *42*, 2537.

[8] a) W. Xing, J. S. Xue, T. Zheng, A. Gibaud, J. R. Dahn, *J. Electrochem. Soc.* **1996**, *143*, 3482; b) J. R. Dahn, T. Zheng, Y. Liu, J. S. Xue, *Science* **1995**, *270*, 590.

[9] a) Y. Sun, Q. Wu, G. Shi, *Energy Environ. Sci.* **2011**, *4*, 1113; b) H. Bai, C. Li, G. Shi, *Adv. Mater.* **2011**, *23*, 1089.

[10] E. Yoo, J. Kim, E. Hosono, H. S. Zhou, T. Kudo, I. Honma, *Nano Lett.* **2008**, *8*, 2277.

[11] a) R. Mukherjee, A. V. Thomas, A. Krishnamurthy, N. Koratkar, *ACS Nano* **2012**, *6*, 7867; b) S. Yang, X. Feng, L. Zhi, Q. Cao, J. Maier, K. Mullen, *Adv. Mater.* **2010**, *22*, 838.

[12] D. Pan, S. Wang, B. Zhao, M. Wu, H. Zhang, Y. Wang, Z. Jiao, *Chem. Mater.* **2009**, *21*, 3136.

[13] X. Yang, J. Zhu, L. Qiu, D. Li, *Adv. Mater.* **2011**, *23*, 2833.

[14] Y. Zhu, S. Murali, M. D. Stoller, K. J. Ganesh, W. Cai, P. J. Ferreira, A. Pirkle, R. M. Wallace, K. A. Cychosz, M. Thommes, D. Su, E. A. Stach, R. S. Ruoff, *Science* **2011**, *332*, 1537.

[15] a) C. Zhang, N. Mahmood, H. Yin, F. Liu, Y. Hou, *Adv. Mater.* **2013**, *25*, 4932; b) W. Ai, L. Xie, Z. Du, Z. Zeng, J. Liu, H. Zhang, Y. Huang, W. Huang, T. Yu, *Sci. Rep.* **2013**, *3*, 2341; c) Z. Du, W. Ai, L. Xie, W. Huang, *J. Mater. Chem. A* **2014**, *2*, 9164; d) N. N. Chai, J. Zeng, K. G. Zhou, Y. L. Xie, H. X. Wang, H. L. Zhang, C. Xu, J. X. Zhu, Q. Y. Yan, *Chem. Eur. J.* **2013**, *19*, 5948.

[16] J. P. Paraknowitsch, A. Thomas, *Energy Environ. Sci.* **2013**, *6*, 2839.

[17] X. Wang, G. Sun, P. Routh, D. H. Kim, W. Huang, P. Chen, *Chem. Soc. Rev.* **2014**, *43*, 7067.

[18] a) A. L. M. Reddy, A. Srivastava, S. R. Gowda, H. Gullapalli, M. Dubey, P. M. Ajayan, *ACS Nano* **2010**, *4*, 6337; b) Y. Liu, X. Wang, Y. Dong, Z. Wang, Z. Zhao, J. Qiu, *J. Mater. Chem. A* **2014**, *2*, 16832.

[19] Z. H. Sheng, L. Shao, J. J. Chen, W. J. Bao, F. B. Wang, X. H. Xia, *ACS Nano* **2011**, *5*, 4350.

[20] H. Wang, T. Maiyalagan, X. Wang, *ACS Catal.* **2012**, *2*, 781.

[21] a) Y. Liu, L. Yuan, M. Yang, Y. Zheng, L. Li, L. Gao, N. Nerngchamnong, C. T. Nai, C. S. S. Sangeeth, Y. P. Feng, C. A. Nijhuis, K. P. Loh, *Nat. Commun.* **2014**, *5*, 5461; b) W. Ai, Z. Z. Du, J. Q. Liu, F. Zhao, M. D. Yi, L. H. Xie, N. E. Shi, Y. W. Ma, Y. Qian, Q. L. Fan, T. Yu, W. Huang, *RSC Adv.* **2012**, *2*, 12204.

[22] a) A. Ranganathan, V. R. Pedireddi, C. N. R. Rao, *J. Am. Chem. Soc.* **1999**, *121*, 1752; b) S. Yagai, S. Mahesh, Y. Kikkawa, K. Unoike, T. Karatsu, A. Kitamura, A. Ajayaghosh, *Angew. Chem. Int. Ed.* **2008**, *47*, 4691.

[23] a) B. V. Lotsch, W. Schnick, *Chem. Eur. J.* **2007**, *13*, 4956; b) G. B. Seifer, *Russ. J. Coord. Chem.* **2002**, *28*, 301; c) E. M. Smolin, L. Rapoport, *Cyanuric Acid and Derivatives, in Chemistry of Heterocyclic Compounds: s-Triazines and Derivatives,* John Wiley & Sons, Inc., Hoboken, NJ **2008**, pp. 17–146.

[24] a) L. Zhang, F. Zhang, X. Yang, G. Long, Y. Wu, T. Zhang, K. Leng, Y. Huang, Y. Ma, A. Yu, Y. Chen, *Sci. Rep.* **2013**, *3*, 1408; b) Y. Yang, K. Wu, R. Pang, X. Zhou, Y. Zhang, X. Wu, C. Wu, H. Wu, S. Guo, *RSC Adv.* **2013**, *3*, 14016; c) L. Lai, J. R. Potts, D. Zhan, L. Wang, C. K. Poh, C. Tang, H. Gong, Z. Shen, J. Lin, R. S. Ruoff, *Energy Environ. Sci.* **2012**, *5*, 7936; d) Y. Yan, Y. X. Yin, S. Xin, Y. G. Guo, L. J. Wan, *Chem. Commun.* **2012**, *48*, 10663.

[25] a) L. Sun, C. Tian, M. Li, X. Meng, L. Wang, R. Wang, J. Yin, H. Fu, *J. Mater. Chem. A* **2013**, *1*, 6462; b) W. Ai, X. Cao, Z. Sun, J. Jiang, Z. Du, L. Xie, Y. Wang, X. Wang, H. Zhang, W. Huang, T. Yu, *J. Mater. Chem. A* **2014**, *2*, 12924; c) W. W. Zhou, J. X. Zhu, C. W. Cheng, J. P. Liu, H. P. Yang, C. X. Cong, C. Guan, X. T. Jia, H. J. Fan, Q. Y. Yan, C. M. Li, T. Yu, *Energy Environ. Sci.* **2011**, *4*, 4954.

[26] a) W. Ai, Z. Du, Z. Fan, J. Jiang, Y. Wang, H. Zhang, L. Xie, W. Huang, T. Yu, *Carbon* **2014**, *76*, 148; b) J. Shang, L. Ma, J. Li, W. Ai, T. Yu, G. G. Gurzadyan, *Sci. Rep.* **2012**, *2*, 792.

[27] a) Z. L. Wang, D. Xu, H. G. Wang, Z. Wu, X. B. Zhang, *ACS Nano* **2013**, *7*, 2422; b) Z. S. Wu, W. Ren, L. Xu, F. Li, H. M. Cheng, *ACS Nano* **2011**, *5*, 5463; c) W. Ai, J. Q. Liu, Z. Z. Du, X. X. Liu, J. Z. Shang, M. D. Yi, L. H. Xie, J. J. Zhang, H. F. Lin, T. Yu, W. Huang, *RSC Adv.* **2013**, *3*, 45.

[28] a) Y. Dong, H. Pang, H. B. Yang, C. Guo, J. Shao, Y. Chi, C. M. Li, T. Yu, *Angew. Chem. Int. Ed.* **2013**, *52*, 7800; b) W. Ai, W. Zhou, Z. Du, Y. Du, H. Zhang, X. Jia, L. Xie, M. Yi, T. Yu, W. Huang, *J. Mater. Chem.* **2012**, *22*, 23439.

[29] a) H. Wang, C. Zhang, Z. Liu, L. Wang, P. Han, H. Xu, K. Zhang, S. Dong, J. Yao, G. Cui, *J. Mater. Chem.* **2011**, *21*, 5430; b) D. Das, S. Kim, K. R. Lee, A. K. Singh, *Phys. Chem. Chem. Phys.* **2013**, *15*, 15128.

[30] a) H. Shimoda, B. Gao, X. P. Tang, A. Kleinhammes, L. Fleming, Y. Wu, O. Zhou, *Phys. Rev. Lett.* **2002**, *88*, 015502; b) H. S. Oktaviano, K. Yamada, K. Waki, *J. Mater. Chem.* **2012**, *22*, 25167.

[31] J. Xu, I. Y. Jeon, J. M. Seo, S. Dou, L. Dai, J. B. Baek, *Adv. Mater.* **2014**, *26*, 7317.

[32] Y. Fang, Y. Lv, R. Che, H. Wu, X. Zhang, D. Gu, G. Zheng, D. Zhao, *J. Am. Chem. Soc.* **2013**, *135*, 1524.